

High Order Slip Flow and Cattaneo-Christov Heat Flux Model for Couple stress fluid

Wubshet Ibrahim*

Department of Mathematics, Ambo University, Ambo, Ethiopia

Email:wubshetib@yahoo.com,Tel.+251911892494

Abebe Tesfaye

Department of Mathematics, Ambo University, Ambo, Ethiopia

Email:abebetesfaye2012@gmail.com,Tel.+251917852782

October 2, 2020

Abstract

Computation of the non-linear convective flow of couple stress nanofluid with the effect of fourth order slip flow, Cattaneo-Christov heat flux model subjected to Biot heating and mass transfer condition over the multi-dimensional stretching surface is presented here. Bvp5c is employed for numerical calculation of velocity, temperature and mass distributions under the control of few governing parameters. The results of current paper were judged with the available works in specific situations and better arrangement has been distinguished. On observing of the flow contours the result indicates that the greater amount of slip of high order the lesser the numerical value of skin friction coefficient, whereas, it is enlarged in value as the magnitude of couple stress parameter rises.

Keywords:Three-dimensional flow; couple stress fluid; Cattaneo-Christov heat and mass flux model; Nanofluid; Fourth order slip flow.

*Corresponding author,E-mail: wubshetib@yahoo.com , Tel +251911892494

Nomenclature

A,B,C,D,E,F,G: constants	Nt : thermophoresis parameter
a,b : are dimensional constant	B_o : non-uniform magnetic field
U_w : surface velocity in the x- direction	N : non-linear convection parameter
V_w : surface velocity in the y- direction	D_B : Brownian diffusion coefficient
U_{slip}, V_{slip} : velocity slip along x-and y-axis	D_T : thermophoretic diffusion coefficient
Sc: Schmidt number	Re_x, Re_y : Reynolds numbers
g : gravitational acceleration	Nu_x : Local Nusselt number
k : couple stress parameter	Sh_x : Local Sherwood number
M: Hartman number	Subscripts
V : velocity vector	∞ : Condition at the free stream
Gr : Grashof number due to temperature	f : Fluid
Pr : Prandtl number	Superscript
Nb: Brownian motion parameter	' : Derivative with respect to η

Greek symbols

\mathfrak{T}_f : liquid at temperature	ζ, \S : are dimensional velocities stream function
\mathfrak{T}_∞ : Ambient temperature	ζ', \S' : are dimensionless velocities
π_c : coefficient of mass transport	ν' : couple stress viscosity
\mathfrak{C}_f : concentration at the wall	σ : electrical conductivity
\mathfrak{C}_∞ : ambient concentration	θ : Dimensionless temperature
\mathfrak{T} : temperature of the fluid	ϕ : Dimensionless concentrationfunction
\mathfrak{C} : is concentration of the fluid	η : similarity variable
Υ, Ψ and Ω : are the velocity components in the x-, y- and z-directions respectively	ξ : thermal diffusivity of fluid
\mathfrak{R} : Velocity ratio parameter	Γ : extra stress tensor
ζ_E : relaxation time parameter heat flux	α : first order slip parameter along x-axis
ζ_C : relaxation time parameter mass flux	β : second order slip parameter along x-axis
λ_1 and μ : are the viscosity coefficients	γ : third order slip parameter along x-axis
η, η' : are the couple stress viscosity coefficients	δ : fourth order slip parameter along x-axis
σ_0 : electric conductivity	φ : first order slip parameter along y-axis
β_T : Thermal expansion coefficient	χ : second order slip parameter along y-axis
β_C : concentration expansion coefficient	ψ : third order slip parameter along y-axis
μ : dynamic viscosity	ω : fourth order slip parameter along y-axis
ρ_f : density of base fluid	λ : buoyancy parameter
ν : kinematic viscosity	βi_1 : Biot number for thermal
ρ : density of fluid	βi_2 : Biot number for concentration
	δ_t : relaxation time parameters of temperature
	δ_c : relaxation time parameters of concentration

1 Introduction

The examination of non-Newtonian fluid due to expanding/shrinking surface with the transport of heat and mass is a long time topic of interest among different researchers. Non-Newtonian fluids of different kind were exist nowadays. A typical example of a non-Newtonian fluid is called as Couple stress. This fluid is the subject of investigation of dozen researchers globally for numerous industrial and scientific applications. Numerous authors have studied couple

stress fluid under different flow configurations. Accordingly, researchers like Srinivasacharya and Kaladhar [1] and Umavathi et al.[2] offered a study on the couple stress fluid with mixed convection and Hall and ion effect under varied physical governing parameters.

Many scholars in the area of fluid dynamics were studied the mentioned fluid with application of vector field like magnetic, electric and others. Hayat et al.[3] and Mahabaleshwar et al.[4] have examined the fluid under consideration due to applied magnetic field past a stretching surface for its varied applications of chemical engineering plants and technological processes. Also, Ramzan [5], Ramzan et al.[6] and Adesanya et al.[7] computed the power of forces due to magnetic field, viscosity and heating impact of a couple stress fluid past bi-directional expanding surface. Also, Ali et al.[8] have presented impact of the time varied magnetic field on transfer of heat for the above indicated fluid over oscillatory extensible scenario. Also, Shit and Roy [9] have discussed the role of obliquely applied magnetic field on the boundary layer flow of couple-stress fluid.

Computation of numerical solution of a couple stress fluid of constant physical parameters has continued by other fluid dynamics researchers taking into account linearity and non-linearity of the surface over which the stretching can takes place. Ghosh et al.[10] and Thammanna et al.[11] have presented a similarity solution of the couple stress fluid over a bi-directional expanding surface with constant applied magnetic field. But, Khan et al.[12] have computed couple stress fluid with the weight of chemical reaction and magnetic field past non-linearly stretching surface. Furthermore, the examination of the couple stress fluid under variable physical condition called heat transmission was carried out by Asad et al.[13].

Jointly, researchers like Ibrahim and Gadisa [14] have employed the heat flux model called Cattaneo-Christove model in examination of couple stress fluid with nanoparticle. Also, analysis of fluid under study subject to variable surface temperature presented by Khan et al.[15]. Also, Ibrahim and Gadisa [16] and Shah et al.[17] have analyzed couple stress- microplar fluid exposed to magnetic region by means of finite element analysis. Further, the suspension of nanoparticle in the couple stress called couple stress nanofluid was examined for the betterment in transmission of heat in the fluid. Therefore, Khan et al.[18] have computationally studied forced and natural convection flow of surface with waving movement and Rehman et al.[19] have studied the stagnation point flow of a couple stress with nanoparticle over non-linearly expanding and porous surface numerically. Furthermore, Hayat et al.[20] have presented melting heat transfer of couple stress fluid and results indicate that couple stress parameter enhance the transmission of heat at the surface. Also, the time varied nanofluid boundary layer flow of couple stress fluid figured as indicated in Awad et al.[21], Umavathi and Sheremet [22] computed heat transfer analysis of couple stress nanofluid. The irreversible process of couple stress fluid with chem-radiation of nanoparticle examined numerically by Ellahi et al.[23] and Sithole et al.[24].

The excellent description of fluid dynamics of external flow of non-Newtonian fluid controlled by different governing parameters has been presented. For instance, Rosali et al.[25] mixed convection flow, Daniel et al.[26] entropy generation analysis, Straughan [27] Cattaneo-Christove heat flux model for thermal convection, Zhao et al. [28] nanofluid past a bi-directional stretching surface, Alam et al.[29] and Palwasha et al.[30] MHD flow has been discussed thoroughly. Furthermore, Dinesh et al.[31] and Malvandi et al.[32] have computed the two-dimensional steady flow of couple stress fluid past a semi-infinite vertical heated plate, non-linearly stretching surface, respectively.

2 Problem Formulation

The following Fig. 1 depicts the flow configuration of steady, laminar multi-dimension non-linear convective flow of couple stress nanofluid with high order slip flow, Christov-Cattaneo diffusion model for heat and mass and condition of convective heat and mass transfer. The Cartesian coordinate system is favored in such a way that x-and y-axes are taken along the stretching surface and z-axes is normal to it. The surface at $z = 0$ in the x-and y-directions having velocities $U_w(x) = ax$ and $V_w(y) = by$, respectively, with $a, b > 0$ as the constants and the flow is in the domain of $z > 0$. Cattaneo-Chiristov heat and mass flux model is fulfilled to inspect the structures of heat and mass transfer of the boundary layer flow.

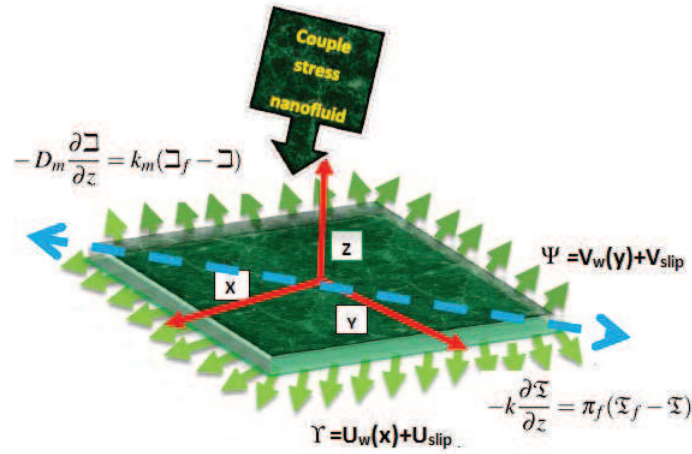


Fig. 1 – Sketch of the flow diagram

The leading equations with Christov-Cattaneo diffusion model for heat and mass transit of the flow problem with the assumptions stated above with allied boundary situations can be given as:

$$\Upsilon \frac{\partial \Upsilon}{\partial x} + \Psi \frac{\partial \Upsilon}{\partial y} + \Omega \frac{\partial \Upsilon}{\partial z} = \nu \frac{\partial^2 \Upsilon}{\partial z^2} - \nu' \frac{\partial^4 \Upsilon}{\partial z^4} - \sigma \frac{B_0^2}{\rho_f} \Upsilon + g\beta_{\vartheta}(\vartheta - \vartheta_{\infty}) + g\beta_c(\vartheta - \vartheta_{\infty})^2 \quad (1)$$

$$\Upsilon \frac{\partial \Upsilon}{\partial x} + \Psi \frac{\partial \Upsilon}{\partial y} + \Omega \frac{\partial \Upsilon}{\partial z} = \nu \frac{\partial^2 \Upsilon}{\partial z^2} - \nu' \frac{\partial^4 \Upsilon}{\partial z^4} - \sigma \frac{B_0^2}{\rho_f} \Upsilon + g\beta_{\vartheta}(\vartheta - \vartheta_{\infty}) + g\beta_c(\vartheta - \vartheta_{\infty})^2 \quad (2)$$

$$\Upsilon \frac{\partial \Psi}{\partial x} + \Psi \frac{\partial \Psi}{\partial y} + \Omega \frac{\partial \Psi}{\partial z} = \nu \frac{\partial^2 \Psi}{\partial z^2} - \nu' \frac{\partial^4 \Psi}{\partial z^4} - \sigma \frac{B_0^2}{\rho_f} \Psi \quad (3)$$

$$\Upsilon \frac{\partial \vartheta}{\partial x} + \Psi \frac{\partial \vartheta}{\partial y} + \Omega \frac{\partial \vartheta}{\partial z} + \zeta_E \Phi_E = \xi \frac{\partial^2 \vartheta}{\partial z^2} + \Gamma [D_B \frac{\partial \vartheta}{\partial z} \frac{\partial \vartheta}{\partial z} + \frac{D_T}{\vartheta_{\infty}} (\frac{\partial \vartheta}{\partial z})^2] \quad (4)$$

$$\Upsilon \frac{\partial \vartheta}{\partial x} + \Psi \frac{\partial \vartheta}{\partial y} + \Gamma [\frac{\partial \vartheta}{\partial z} + \zeta_C \Phi_C] = D_B \frac{\partial^2 \vartheta}{\partial z^2} + \frac{D_T}{\vartheta_{\infty}} \frac{\partial^2 \vartheta}{\partial z^2} \quad (5)$$

The boundary conditions are

$$\Upsilon = \Upsilon_w(x) + \Pi_1, \Psi = \Psi_w(y) + \Pi_2, \Omega = 0 \quad \text{at} \quad z = 0,$$

$$-k \frac{\partial \mathfrak{T}}{\partial z} = \pi_f(\mathfrak{T}_f - \mathfrak{T}), -D_m \frac{\partial \mathfrak{C}}{\partial z} = k_m(\mathfrak{C}_f - \mathfrak{C}) \quad \text{at } z = 0, \\ \Upsilon \rightarrow 0, \Psi \rightarrow 0, \mathfrak{T} \rightarrow \mathfrak{T}_\infty, \mathfrak{C} \rightarrow \mathfrak{C}_\infty \quad \text{as } z \rightarrow \infty \quad (6)$$

Eqs.(1)-(5) are equations from conservation laws of 3D non-linearly convectively flow of couple-stress nanofluid with Christov-Cattaneo heat and mass flux model. In the above equations Υ , Ψ and Ω denote the velocity components in the x-, y- and z-directions respectively, $\nu(= \frac{\mu}{\rho_f})$ represents the kinematic viscosity, μ stands for dynamic viscosity, ρ_f symbolizes the density of base fluid, ν' denotes the couple stress viscosity, σ denotes the electrical conductivity, B_0 stands for magnetic field strength, \mathfrak{T} denotes the temperature, \mathfrak{C} denotes the nanoparticles concentration, \mathfrak{T}_f liquid at temperature, \mathfrak{C}_f concentration at the wall, \mathfrak{T}_∞ represents the ambient values of temperature and \mathfrak{C}_∞ represents the ambient values of concentration, β_T the thermal expansion coefficient, β_C the concentration expansion coefficient, g is gravitational acceleration, $\xi = \frac{k}{(\rho c)_f}$ signifies the thermal diffusivity of fluid, D_B stands for Brownian diffusion coefficient, D_T denotes the thermophoretic diffusion coefficient, ζ_E stands the thermal relaxation time, ζ_C represents the concentration relaxation time, $\Gamma = \frac{(\rho c)_p}{(\rho c)_f}$ represents the extra stress tensor, respectively. Π_1 and Π_2 are the slip velocity at the surface x-and y-directions which are given as the follows:

$$\Pi_1 = A \frac{\partial \Upsilon}{\partial y} + B \frac{\partial^2 \Upsilon}{\partial y^2} + C \frac{\partial^3 \Upsilon}{\partial z^3} + D \frac{\partial^4 \Upsilon}{\partial z^4}, \Pi_2 = E \frac{\partial \Psi}{\partial y} + F \frac{\partial^2 \Psi}{\partial y^2} + G \frac{\partial^3 \Psi}{\partial z^3} + H \frac{\partial^4 \Psi}{\partial z^4} \quad (7)$$

where A,B,C,D,E,F,G and H are fixed parametric constants. Similarity restorations of the following type are used to make simpler the mathematical formula of the flow fields as described in (Ramzan et al.[6] and Ibrahim[33]).

$$\Upsilon = ax\zeta'(\eta), \Psi = by\xi'(\eta), \Omega = -\sqrt{av}(\zeta(\eta) + \xi(\eta)), \eta = \sqrt{\frac{a}{\nu}}z \quad (8)$$

$$\theta(\eta) = \frac{\mathfrak{T} - \mathfrak{T}_\infty}{\mathfrak{T}_f - \mathfrak{T}_\infty}, \phi(\eta) = \frac{\mathfrak{C} - \mathfrak{C}_\infty}{\mathfrak{C}_f - \mathfrak{C}_\infty} \quad (9)$$

incompressibility condition (1) is now satisfied and (2) - (6) the overall non - dimensional equations are :

$$\zeta''' + (\zeta + \xi)\zeta'' - k\zeta^{(5)} - \zeta'^2 - M^2\zeta' + \lambda\theta(1 + N\theta) = 0 \quad (10)$$

$$\xi''' + (\zeta + \xi)\xi'' - k\xi^{(5)} - \xi'^2 - M^2\xi' = 0 \quad (11)$$

$$\theta'' + Pr(\zeta + \xi)\theta' + PrNb\theta'\phi' + PrNt\theta'^2 - \delta_t Pr(\theta'' + \theta')(\zeta + \xi)^2 = 0 \quad (12)$$

$$\phi'' + \frac{N_t}{N_b}\theta'' + Sc(\zeta + \xi)\phi' - \delta_c Sc[(\zeta + \xi)^2\phi'' + (\zeta + \xi)(\zeta' + \xi')\phi'] = 0 \quad (13)$$

The renovated situation at edge are:

$$\zeta(\eta) = \xi(\eta) = 0, \zeta'(\eta) = 1, \xi'(\eta) = \mathfrak{K}, \theta'(\eta) = -\beta_{i1}(1 - \theta(\eta)), \phi'(\eta) = -\beta_{i2}(1 - \phi(\eta)), \\ \zeta'(\infty) \rightarrow 0, \zeta''(\infty) \rightarrow 0, \zeta'''(\infty) \rightarrow 0, \xi'(\infty) \rightarrow 0, \xi''(\infty) \rightarrow 0, \xi'''(\infty) \rightarrow 0, \theta(\infty) \rightarrow 0, \phi(\infty) \rightarrow 0 \quad (14)$$

the slip with x-and y-directions are:

$$\zeta'(\eta) = 1 + \alpha\zeta''(\eta) + \beta\zeta'''(\eta) + \gamma\zeta''''(\eta) + \delta f^{(5)}(\eta) \quad \text{at } \eta = 0 \quad (15)$$

$$\S'(\eta) = \mathfrak{K} + \varphi \S''(\eta) + \chi \S'''(\eta) + \psi \S''''(\eta) + \omega \S^{(5)}(\eta) \quad \text{at} \quad \eta = 0 \quad (16)$$

where ζ' , \S' , θ , ϕ are non-dimensionalized flow field along x- and y-axis, temperature, and particle concentration respectively. η is the similarity variable, $\alpha = \varphi$, $\beta = \chi$, $\gamma = \psi$ and $\delta = \omega$ first, second, third and fourth order slips respectively, Prandtl number Pr, buoyancy ratio N, Brownian motion Nb, Lewis number Le, Schmidt number Sc, thermophoresis parameter Nt, δ_t is parameter for relaxation time for temperature, δ_c is parameter for relaxation time for particle concentration, Bi_1 Biot number for temperature, Bi_2 Biot number for particle concentration, M Hartmann number, k couple stress parameter, \mathfrak{K} velocity ratio parameter, Gr stands for Grashof number, respectively. These parameters are defined as follows:

$$\begin{aligned} \alpha &= A\sqrt{\frac{a}{\Psi}}, \beta = B\frac{a}{\Psi}, \gamma = C\sqrt{\frac{a^3}{\Psi}}, \delta = D\frac{a^2}{v^2}; \varphi = E\sqrt{\frac{a}{\Psi}}, \chi = F\frac{b}{a}, \psi = G\sqrt{\frac{a^3}{\Psi}}, \omega = H\frac{a^2}{v^2}, \mathfrak{K} = \frac{b}{a}, \\ Pr &= \frac{\Psi}{\xi}, \lambda = \frac{Gr}{Re_x}, Nb = \Gamma\left(\frac{D_B(\mathfrak{I}_f - \mathfrak{I}_\infty)}{\Psi}\right), Nt = \frac{D_T}{\mathfrak{I}_\infty} \frac{\mathfrak{I}_f - \mathfrak{I}_\infty}{\Psi} \delta_t = \zeta_E a, \delta_c = \zeta_C a, Sc = PrLe, k = v' \frac{a}{\Psi}, \\ M &= \left(\frac{\sigma B_0^2}{a \rho_f}\right), Re_x = \frac{ax^2}{\Psi}, Gr = \frac{g\beta_T(\mathfrak{I}_f - \mathfrak{I}_\infty)}{v^2} y^3, Re_x^2 = \frac{a^2 x^4}{v^2}, Re_y^2 = \frac{a^2 y^4}{v^2}; N = \frac{g\beta_c(\mathfrak{I}_f - \mathfrak{I}_\infty)}{\beta_T} \end{aligned} \quad (17)$$

Skin-Friction coefficient $C_{\zeta x}$ and $C_{\S y}$ local-Nusselt number Nu_x and the local-Sherwood number Sh_x .

$$C_{\zeta x} = \frac{\tau_{wx}}{\rho u_{wx}^2} \text{ and } C_{\S y} = \frac{\tau_{wy}}{\rho v_{wy}^2}, Nu_x = \frac{xq_w}{k(\mathfrak{I}_f - \mathfrak{I}_\infty)}, Sh_x = \frac{xh_w}{k(\mathfrak{I}_f - \mathfrak{I}_\infty)} \quad (18)$$

where the wall shear stress τ_{wx} and τ_{wy} , wall heat flux q_w , and wall mass flux h_w are given by:

$$\tau_{wx} = \Psi \frac{\partial \Upsilon}{\partial z} - v' \frac{\partial^3 \Upsilon}{\partial z^3}, \tau_{wy} = v \frac{\partial \Psi}{\partial z} - v' \frac{\partial^3 \Psi}{\partial z^3}, q_w = -k \left(\frac{\partial \mathfrak{I}}{\partial z} \right)_{z=0}, h_w = -D_B \left(\frac{\partial \mathfrak{I}}{\partial z} \right)_{z=0}, \quad (19)$$

Using above equations (18) and (19) and reduced to:

$$\sqrt{Re} C_{\zeta x} = \zeta''(0) - k \zeta''''(0), \sqrt{Re} C_{\S y} = \S''(0) - k \S''''(0), \frac{Nu_x}{\sqrt{Re_x}} = -\theta'(0), \frac{Sh_x}{\sqrt{Re_x}} = -\phi'(0) \text{ at } \eta = 0 \quad (20)$$

It is seen to that $Re_x = \frac{U_w}{\Psi}$ and $Re_y = \frac{V_w}{\Psi}$ represent the local Reynolds numbers.

3 Numerical Solution

Eqs. (10)-(13) with attached boundary conditions Eq. (10) are actual multiple nonlinear ODEs whose exact results are dreadful. Hence, numerical algorithm should be employed to get the solution of these equations. In this computation the MATLAB R2019a bvp5c solver is utilized to grasp the numerical solution for (10)-(13) and these equations are condensed to:

$$\begin{aligned} y_1 &= \zeta, y_2 = \zeta', y_3 = \zeta'', y_4 = \zeta''', y_5 = \zeta'''' , y'_5 = \zeta^{(5)}, y_6 = \S, y_7 = \S', y_8 = \S'', y_9 = \S''', \\ y_{10} &= \S'''' , y'_{10} = \S^{(5)}, y_{11} = \theta, y_{12} = \theta', y'_{12} = \theta'', y_{13} = \phi, y_{14} = \phi', y'_{14} = \phi'' \end{aligned} \quad (21)$$

The compressed form of (21) is specified as follows:

$$\begin{pmatrix} y_1' \\ y_2' \\ y_3' \\ y_4' \\ y_5' \\ y_6' \\ y_7' \\ y_8' \\ y_9' \\ y_{10}' \\ y_{11}' \\ y_{12}' \\ y_{13}' \\ y_{14}' \end{pmatrix} = \begin{pmatrix} y_2 \\ y_3 \\ y_4 \\ y_5 \\ (\frac{1}{k})(y_4 + (y_1 + y_6)y_3 - y_2^2 - M^2 y_2) + \lambda y_0(11)(1 + N y_0(11)) \\ y_7 \\ y_8 \\ y_9 \\ y_{10} \\ (\frac{1}{k})(y_9 + (y_1 + y_6)y_8 - y_7^2 - M^2 y_7) \\ y_{12} \\ \frac{\delta_t P_r y_{10}(y_1 + y_6)^2 - P_r N_b y_{10} y_{12} - P_r N_t y_{10}^2 - P_r (y_1 + y_6) y_{10}}{1 - \delta_t P_r (y_1 + y_6)^2} \\ y_{14} \\ \frac{-\frac{N_t}{N_b} y_{10}' - S c (y_1 + y_6) y_{12} + \delta_c S c (y_1 + y_6) (y_2 + y_6) y_{12}}{1 - \delta_c S c (y_1 + y_6)^2} \end{pmatrix} \quad (22)$$

Corresponding conditions at the boundary are:

$$\begin{pmatrix} y_1(0) \\ y_2(0) \\ y_6(0) \\ y_7(0) \\ y_{12}(0) \\ y_{14}(0) \\ y_{inf}(2) \\ y_{inf}(3) \\ y_{inf}(4) \\ y_{inf}(7) \\ y_{inf}(8) \\ y_{inf}(9) \\ y_{inf}(11) \\ y_{inf}(13) \end{pmatrix} = \begin{pmatrix} 0 \\ 1 + \alpha y_0(3) + \beta y_0(4) + \gamma y_0(5) + \delta (1/k)((y_0(4) + y_0(3))(y_0(1) + y_0(6)) - (y_0(7))^2 - (M^2) y_0(7)) + \lambda y_0(11)(1 + N y_0(11)) \\ 0 \\ \mathfrak{K} + \varphi y_0(8) + \chi y_0(9) + \psi y_0(10) + \omega (1/k)((y_0(9) + y_0(8))(y_0(1) + y_0(6)) - (y_0(2))^2 - (M^2) y_0(2))) \\ -B i_1 (1 - y_0(11)) \\ -B i_2 (1 - y_0(13)) \\ 0 \\ 0 \\ 0 \\ 0 \\ 0 \\ 0 \\ 0 \\ 0 \end{pmatrix} \quad (23)$$

4 Outcomes and Discussion

In this consequence tied interrelated equations (10)-(13) along conforming boundary conditions (2) were numerically computed for speckled values of leading constraints using `bvp5c` solver in MATLAB R2019a. When the values of the parameters taken as $k = 0.02$, $\lambda = 0.5$, $N = 0.5$, $Pr = 0.71$, $M = Nb = Nt = 0.1$, $\mathfrak{K} = 0.2$, $Sc = 0.8$, $\beta_1 = \beta_2 = 0.5$, $\delta t = 0.3$, $\delta c = 0.2$, $\alpha = \beta = \gamma = \delta = \varphi = \chi = \psi = \omega = 1$ the numerical output were gained.

The numerical solutions were exhibited in the forms of pictorial tables and graphs. Fig. 2 was plotted for illustration of influence of the couple stress parameter k on velocity along x -axis. Increasing the rate of couple stress parameter induces the dimensionless velocity along $\zeta'(\eta)$ to increase up to $\eta = 3$ distance away from the body of the sheet and then maintain the

convergence to zero as $\eta \rightarrow \infty$. Further an increment in velocity associated with an increment in nonlinear convection parameter N as shown Fig. 3. Fig. 4 characterize that weight of fourth order slip parameter δ on velocity graph along x-axis and it shows that $\zeta'(\eta)$ is decreasing initially up to $\eta \approx 2$ and then it converges to zero as η increases to some larger value. Physically, buoyancy ratio parameter N accelerate the deformation of fluid particles, consequently flow field enhanced and velocity boundary layer thickness as well but fourth order slip δ display opposite scenario. The characteristics of buoyancy parameter λ on non-dimensional velocity oriented in x-axis $\zeta'(\eta)$ is exhibited in Fig. 5 and it pinpoints that $\zeta'(\eta)$ is helped to grow by buoyancy parameter λ . Thus, an enhancement in buoyancy parameter λ , causes a depilation in viscous force as a result fluid motion will accelerates. Normally, buoyancy parameter λ favors velocity of flow. The flow field graph $\zeta'(\eta)$ for few value of third order slip parameter γ is delivered in Fig. 6. The property illustrated in the figure confirms that $\zeta'(\eta)$ is along with γ . Moreover, the thickness of boundary stratum is thickened and flow field is improved as the value of γ is boosting in the absolute value. Physically a reduction of friction force associated with an increase in the slip factor which allows more fluid to slip past the sheet and the flow field accelerates.

The result identified that the magnetic field parameter (M) lessen the velocity of the flow along y-axis $\xi'(\eta)$ as demonstrated in Fig. 7. It is found that both the y-component velocity and boundary layer stratum were greatly lessen when the Hartman number M was intensified. The retarding effect was shown by the Lorentz force (body force) on the velocity graphs. Hence, the fluid motion was opposed by the Lorentz force, consequently, the velocity of the fluid decreases.

Fig. 8 characterize the power of velocity ratio parameter \aleph on the velocity components $\xi'(\eta)$. $\xi'(\eta)$ is grown by escalation of the amount of parameter \aleph . In fact, proliferation in \aleph due to the rate constant subject to the rate of velocity along x-axis to the y-component of velocity. Therefore, $\xi'(\eta)$ proliferates as the amount of c increases i.e. when the velocity along y-axis less than velocity along x-axis greater. Fig. 9 is sketched to specify the influence of few values of forth order slip parameter ω on the velocity along y-components $\xi'(\eta)$. Accordingly the velocity component $\xi'(\eta)$ was lessen when the value of fourth order slip parameter ω is upsurge. Hence, $\xi'(\eta)$ was grown as third order slip improved, but it decreased as fourth order slip parameter increased.

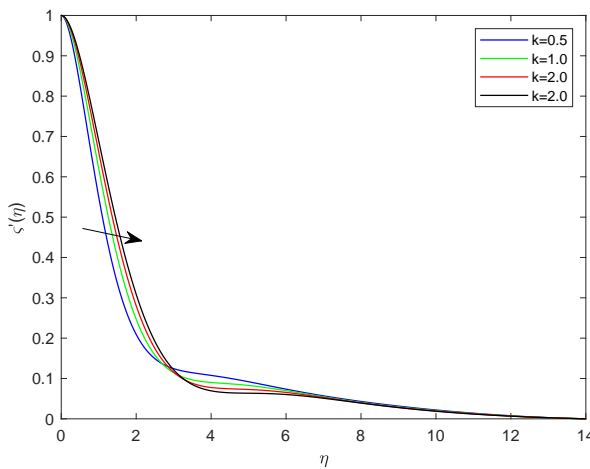


Fig. 2 – Power of couple stress parameter on velocity

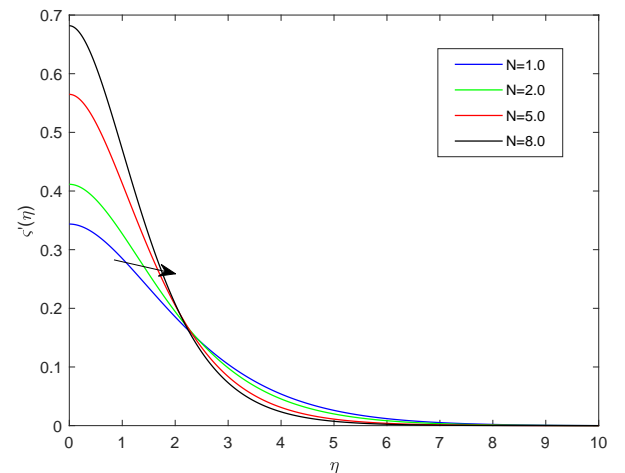


Fig. 3 – Impacts of non-linear convection parameter on velocity

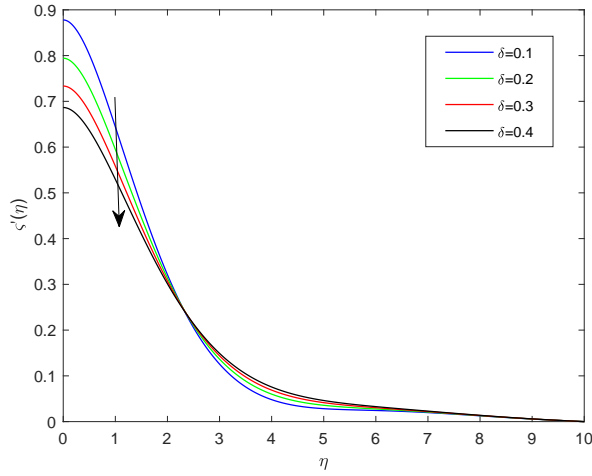


Fig. 4 – Influences of fourth order slip parameter for $\zeta'(x)$ velocity

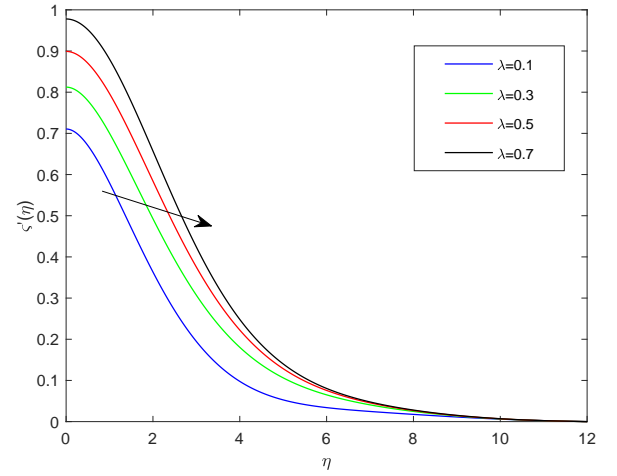


Fig. 5 – Power of buoyancy parameter on velocity

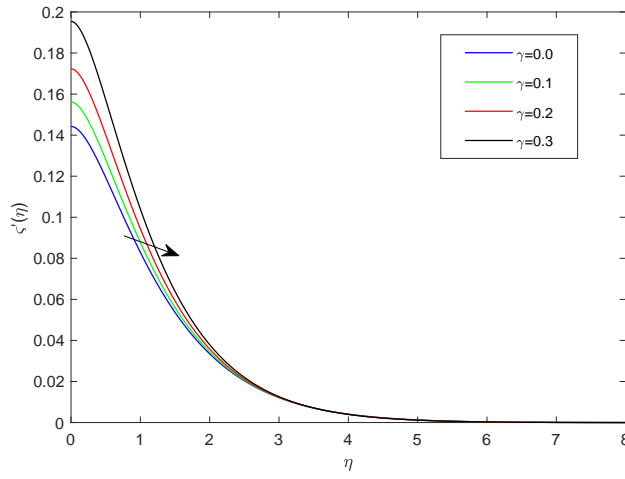


Fig. 6 – Third order slip parameter on fluid velocity

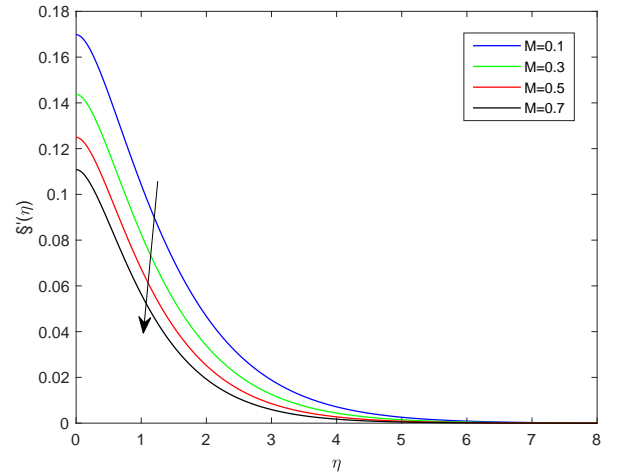


Fig. 7 – Properties of Hartman number for $\zeta'(y)$ on fluid velocity

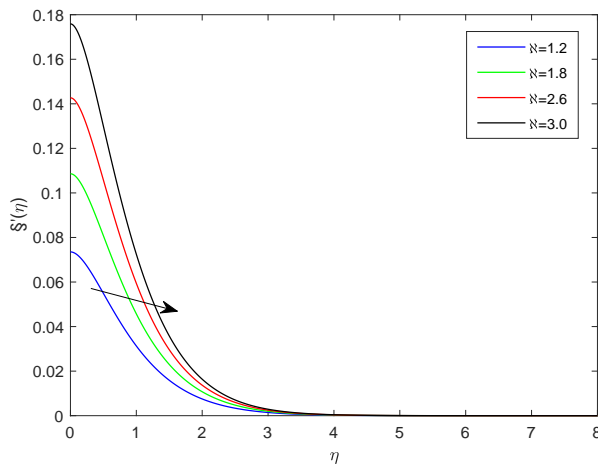


Fig. 8 – Velocity ratio parameter \aleph on fluid velocity

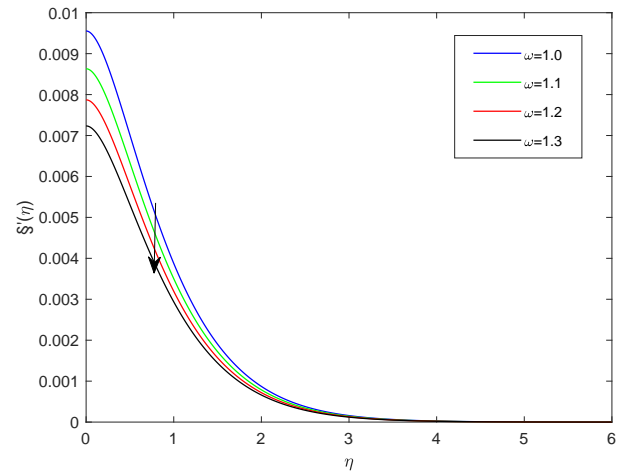


Fig. 9 – Fourth order slip parameter on $\zeta'(y)$ velocity

The power of the leading parameters on temperature graphs is presented in this section of

the paper. Accordingly, Fig. 10 and Fig. 11 were schemed to portrait the weight of direction less motions of the particles of fluid (Brownian motion) parameter and thermophoresis parameter on temperature field. It is analyzed that temperature distribution are favored by larger values of both parameters. A random motion of the fluid particles increases as Brownian motion parameter Nb increases, which results in more collisions of the fluid particles as a result in generation of more kinetic energy of the particle, lastly more heat is produced in the boundary layer. Hence both temperature profile and the thermal boundary layer thickness were grown.

The power of Biot number Bi_1 on temperature graph is displayed in Fig. 12. Physically, the ratio of convective at the surface to conduction with in the surface of the body is Biot number Bi_1 . Weak conduction on the surface implies big Biot number and weak convection implies the small Biot number. The temperature graph against Biot number Bi_1 also foreseen this behavior. Further, Biot number Bi_1 heighten the fluid temperature.

Fig. 13 clarifies the inspiration of thermal relaxation parameter δ_t on temperature graph. It is illustrated that an improvement in the value of thermal relaxation parameter and Fick model of mass diffusion show an increment in the behavior for temperature field and thermal boundary layer thickness of the study. The amount of heat transited from the surface to the fluid depends on the thermal relaxation parameter. Hence an increment in thermal relaxation parameter resulted in small transit of heat. Consequently, a decline in temperature distribution observed in the temperature field. Fig. 14 displays the weight of buoyancy ratio parameter N on temperature graph. From the figure, the temperature of the fluid is minimized by augmenting the value of buoyancy ratio parameter N . Mathematically thermal buoyancy parameter is explained as the ratio of buoyancy to viscous forces in the boundary layer. Therefore, adding its value lessen the viscosity of the couple stress nano fluid and resulted in the reduction in distribution of temperature.

Fig. 15 denotes the temperature profiles graph under the variation of Prandtl number parameter Pr . It shows that the weight of Prandtl number is to minimize both temperature and themal boundary stratum. Prandtl number and thermal diffusivity are inversely related.

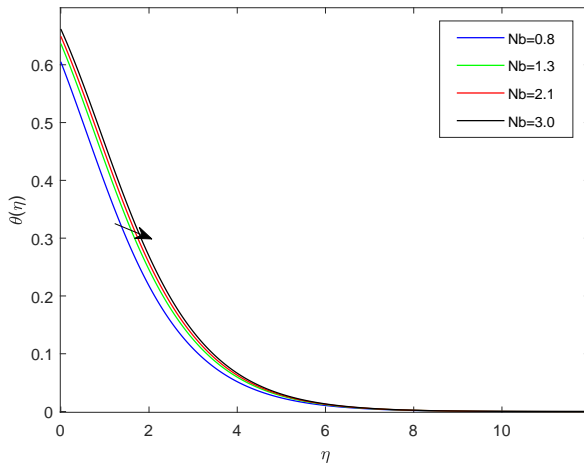


Fig. 10 – Brownian motion parameter Nb on temperature profile

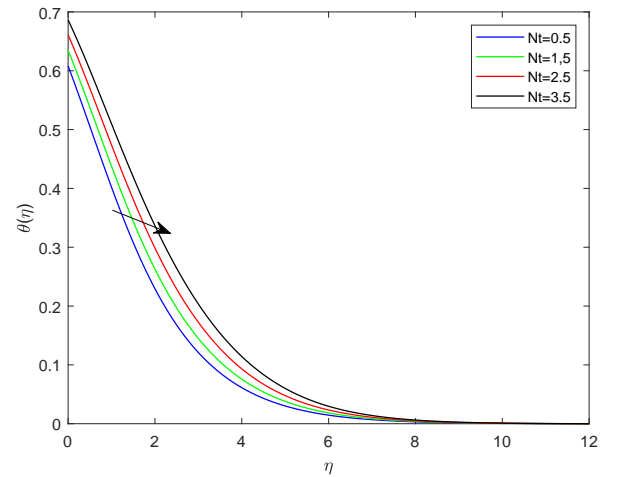


Fig. 11 – thermophoresis parameter Nt on temperature profile

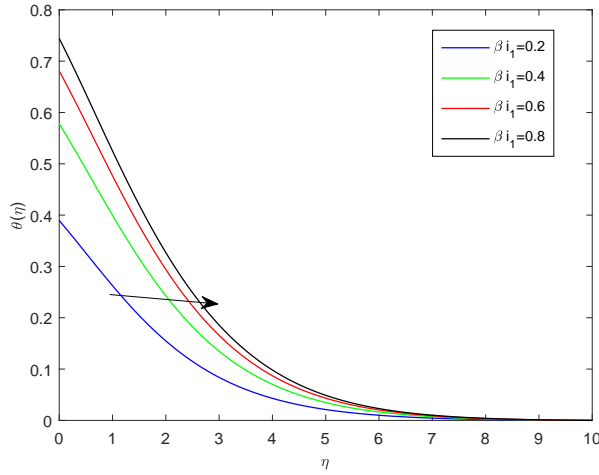


Fig. 12 – Properties of Biot number Bi_1 on temperature profile

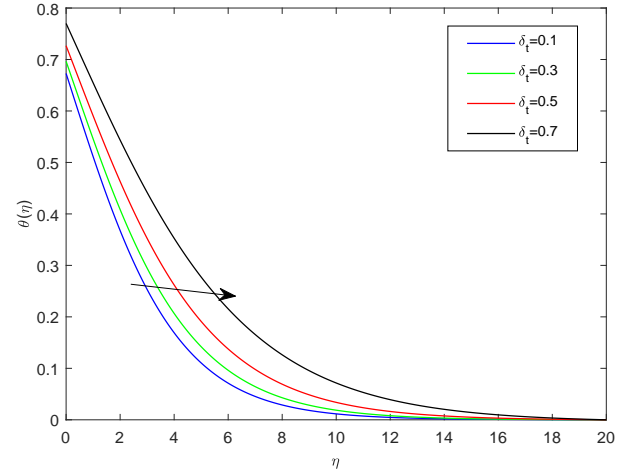


Fig. 13 – Thermal relaxation parameter δ_t on fluid temperature profile

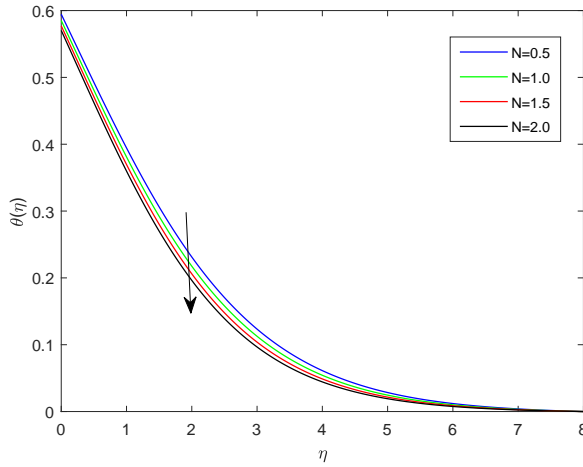


Fig. 14 – Belongings of buoyancy parameter on fluid temperature profile

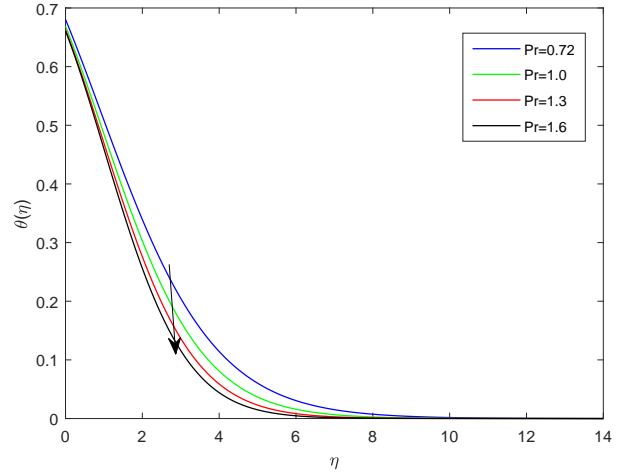


Fig. 15 – Impacts of Prandtl number on particle temperature profile

The following paragraphs pinpoint the power of some governing parameters on concentration graphs. Therefore, Fig. 16 sketched to signify the weight of thermal buoyancy parameter λ on concentration graph. It articulates that intensification in thermal buoyancy parameter λ resulted in lessen in both the concentration and concentration boundary layer thickness. The result suggested that higher values of thermal buoyancy parameter implies to stronger buoyancy force and this force is caused drop of concentration boundary layer comprehensiveness.

Fig. 17 demonstrates the sketch of nanoparticles concentration distribution for few values of couple stress parameter k . Weaker nanoparticles concentration distributions and thin nanoparticles concentration boundary layer thicknesses is a result of the great the values of couple stress parameter. In addition, concentration graph for few values of Schmidt number Sc is illustrated in Fig. 18. It indicate that concentration and its boundary layer thickness are significantly minimal for huge values of Schmidt number Sc . Physically, Schmidt number Sc is the quotient of diffusivity of momentum to mass. Association of Brownian motion parameter Nb with concentration distribution is established in Fig. 19. In this computation, if the value of Nb are get higher than the concentration boundary layer thickness is depreciating. Because for large value of Nb , the arbitrary motion and also impact of the nanoparticles fluids are high which decreases the concentration of the fluid.

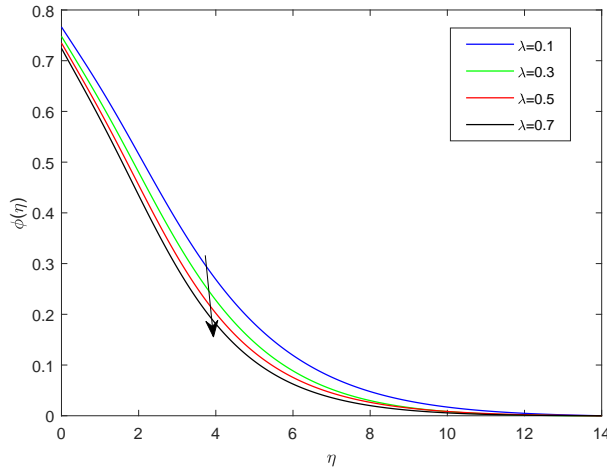


Fig. 16 – Influences of buoyancy parameter λ on particle concentration profile

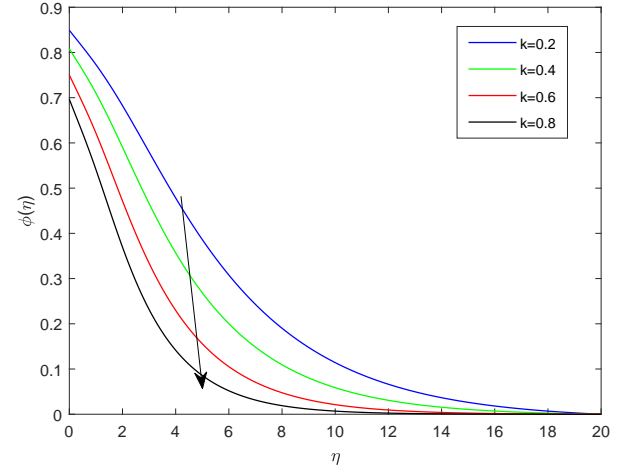


Fig. 17 – Effects of couple stress parameter K on concentration profile

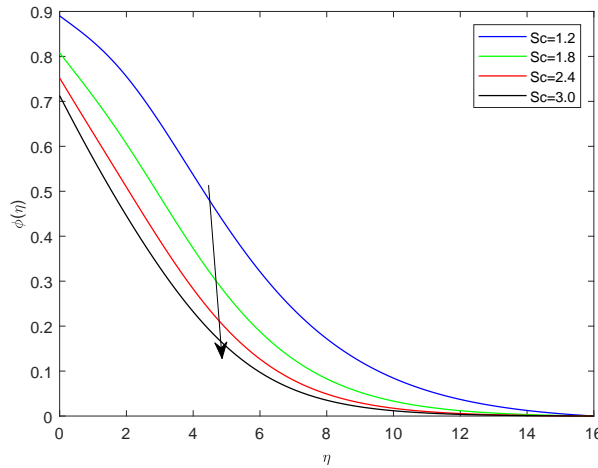


Fig. 18 – Influences of Schmidt number on concentration profiles

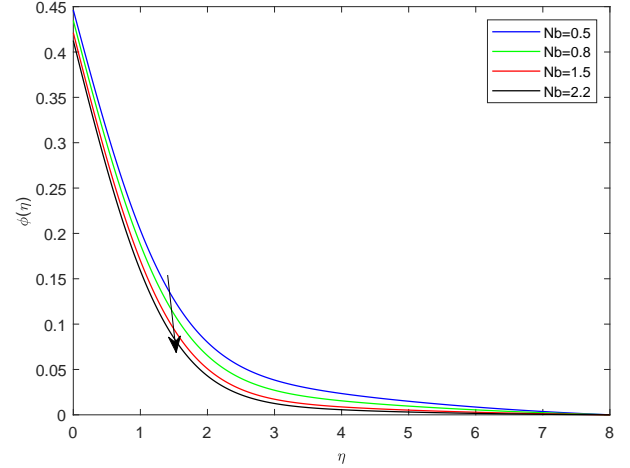


Fig. 19 – Properties of Brownian motion on concentration profile

Features of third order slip parameter γ and Hartman number M on skin friction coefficient along x-axis ($\zeta''(0)$) graph are exhibited in Fig. 20. The magnitude of the skin friction coefficient seems to constantly increasing for higher values of third order slip γ and Hartman numbers M. Characteristics of fourth order slip δ and λ on skin friction coefficient along x-axis $\zeta''(0)$ graph are displayed in Fig. 21. The skin friction coefficient increases for higher values of δ while increase in increase in λ . The effect of fourth order slip ω and λ on skin friction coefficient along y-axis $\xi'(0)$ graph are displayed in Fig. 22. The magnitude of the skin friction coefficient for $\sqrt{Re}C_{\xi y}$ increases for higher values of fourth order slip ω and buoyancy parameter λ . Fig. 23 expresses the behavior of k and M on local Nusselt number $Nu_x = -\theta'(0)$. It is examined that local Nusselt number $Nu_x = -\theta'(0)$ increases for higher values of M while it reduces with an enlargement in k . Fig. 24 displays the behavior of Nb and Hartman numbers M on the variation of local Nusselt number $Nu_x = -\theta'(0)$. It is indicated in the graph that of local Nusselt number $Nu_x = -\theta'(0)$ rises for big values of Nb but it get reduced with the growth in Hartman numbers M. Fig. 25 interprets the influence of thermal biot-number parameter $\beta_1 l$ and thermophoresis parameter Nt on local Nusselt number. As

seen from the graph, local Nusselt number $Nu_x = -\theta'(0)$ magnifies with an enhancement in thermal biot-number β_i parameter along with an increment in the values of thermophoresis parameter Nt .

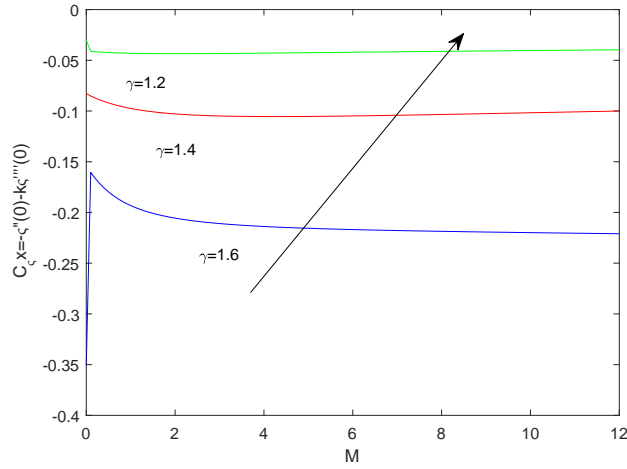


Fig. 20 – Influences of third order slip parameter γ on skin friction coefficient

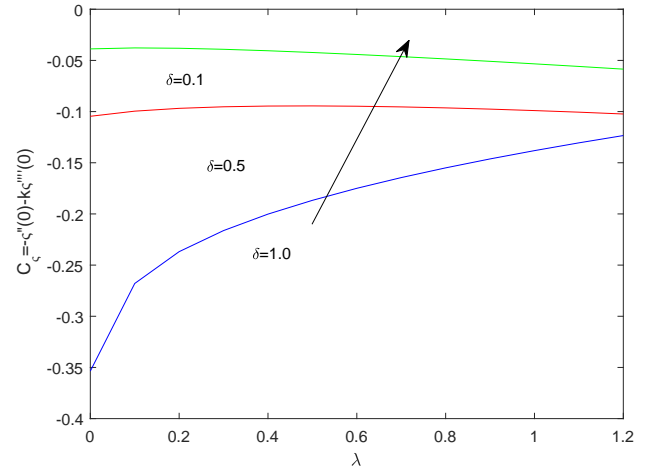


Fig. 21 – Effect of fourth order slip δ $\zeta'(x)$ on coefficient skin friction

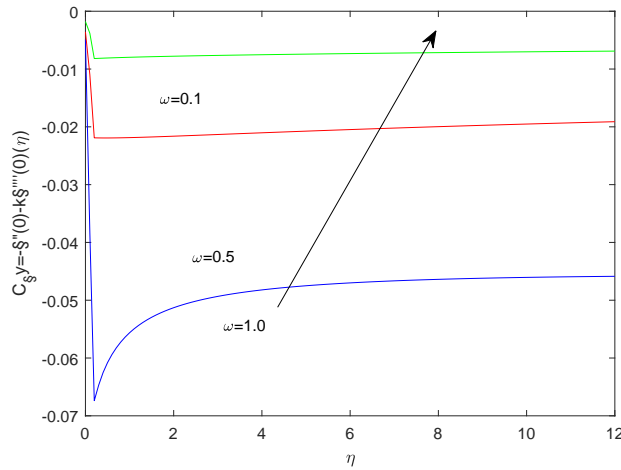


Fig. 22 – Impacts of fourth order slip ω for $\zeta'(y)$ on coefficient skin friction

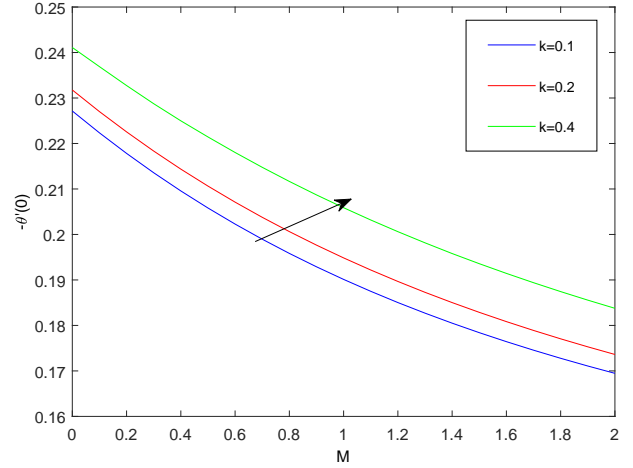


Fig. 23 – Influences of couple stress parameter k on heat transfer rate

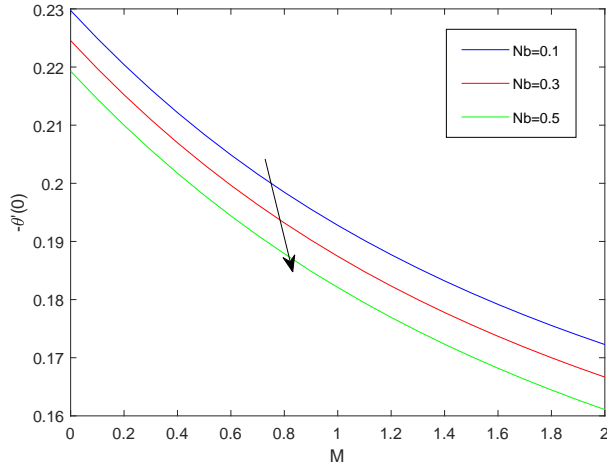


Fig. 24 – Effects of Brownian motion parameter Nb rate of heat transfer

Table 1 illustrates the comparison of $\zeta''(0)$ and $\xi''(0)$ with the preceding results in the literature. The table shows that the present result is in good harmony with similar paper in the area. Table 2 and Table 3 display the impact of different number of λ , γ , and δ on $\zeta''(0)$ and $g''(0)$. The rise in the values of λ , γ , and δ resulted in the rise of the values of the local skin-friction coefficients along both x- and y- directions. However, an enlargement in the magnitude of k , N , \aleph , and ω , cause a deduction in local skin-friction coefficient along x- and y- directions but the values of M cause a reduction in local skin-friction coefficient along x-axis and enlarge in the y-axis.

In addition, observing from Table 4 that, an increased in the values of K , Nb , and β_{i2} , causes a growth in the values of Sherwood number. On the contrary, increasing the values of Nt , Pr , δ_c and β_{i1} , results diminution of Sherwood number. Comparatively, the effect of the parameters was more on the temperature and nanoparticles concentration profiles.

Judgment of the local skin-friction coefficient $-\zeta''(0) - k\zeta''''(0)$ and $-\xi''(0) - k\xi''''(0)$ of Present result with (Ramzan et al. [6]) is very good agreement, (see table) (1).

Table 1 – Judgment of $\zeta''(0)$ and $\xi''(0)$ when $k=0.00001, M=0.0$ when $Pr =, Nb =, Nt =, \beta_{i1} =, \beta_{i2} =, \delta t =, \delta c = 0.00001$ but other parameters are zero

\aleph	(Ramzan et al[6]) $-\zeta''(0)$	$Pv - \zeta''(0)$	(Ramzan et al[6]) $-\xi''(0)$	$Pv - \xi''(0)$
0.0	1.0000	1.000108	0.00000	0.000000
0.1	1.0203	1.020342	0.06684	0.066843
0.2	1.0395	1.039558	0.14874	0.148727
0.3	1.0580	1.058001	0.24336	0.243344
0.4	1.0758	1.075820	0.34921	0.349188
0.5	1.0931	1.093114	0.46520	0.465181
0.6	1.1099	1.109955	0.59053	0.590503
0.7	1.1264	1.126396	0.72454	0.724505
0.8	1.1425	1.142478	0.86668	0.866656
0.9	1.1582	1.158234	1.01650	1.016512
1.0	1.1737	1.173693	1.17370	1.173693

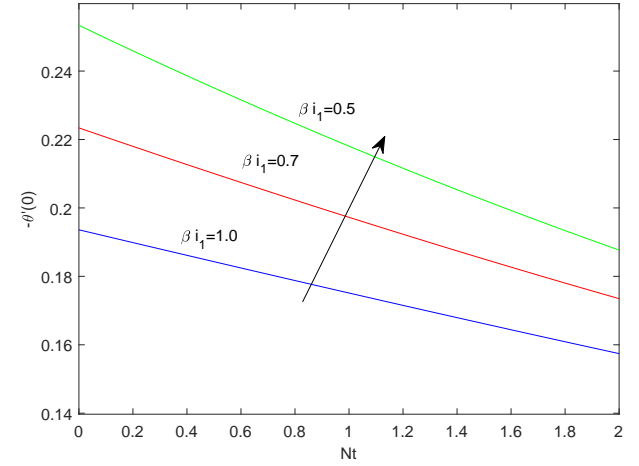


Fig. 25 – Influences of thermal biot-number parameter on rate of heat transfer

where Pv is present value.

Table 2 – Local Skin-friction coefficients via $k, \lambda, N, \gamma, \delta$ when $Pr=0.1, Nb = 0.1, Nt = 0.2, \aleph = 0.2, Sc = 0.8, \beta_1 = \beta_2 = 0.5, \delta_t = 0.3, \delta_c = 0.2, \alpha = 0.2, \beta = 0.4, \phi = 0.2, \chi = 0.3, \psi = 0.2, \omega = 0.2$

k	λ	N	γ	δ	$-\zeta''(0)$	$-\xi''(0)$
0.02	0.5	0.5	0.2	0.3	-0.011859	-0.001554
0.1					-0.017409	-0.018642
0.3					-0.304354	-0.074795
0.5					-0.542342	-0.128415
0.02	0.6	0.5	0.2	0.3	-0.013161	-0.001554
	0.7				-0.011479	-0.001558
	0.9				-0.011349	-0.001561
0.02	0.5	0.6	0.2	0.3	-0.016113	-0.001552
		0.7			-0.016257	-0.001552
		0.9			-0.016402	-0.001553
0.02	0.5	0.5	0.4	0.3	-0.009044	-0.001553
			0.6		-0.008046	-0.001296
			0.8		-0.005148	-0.001106
0.02	0.5	0.5	0.2	0.5	-0.005601	-0.001553
				0.7	-0.004561	-0.001553
				0.9	-0.003995	-0.001553

Table 3 – The $-\zeta''(0) - \xi''(0)$ via $k, M, \aleph, \phi, \chi, \psi, \omega$ when $\lambda = 0.5, N = 0.5, Pr=0.1, Nb = 0.1, Nt = 0.2, Sc = 0.8, \beta_1 = \beta_2 = 0.5, \delta_t = 0.3, \delta_c = 0.2, \alpha = 0.2, \beta = 0.4, \gamma = 0.2, \delta = 0.1, \phi = 0.3, \chi = 0.2$

k	M	\aleph	ψ	ω	$-\zeta''(0)$	$-\xi''(0)$
0.02	0.8	0.2	0.3	0.4	-0.014501	-0.001551
0.1					-0.155875	-0.017996
0.2					-0.401127	-0.048557
0.3					-0.648487	-0.082560
0.02	0.9	0.2	0.3	0.4	-0.014967	-0.001549
	1.0				-0.015402	-0.001548
	1.2				-0.016153	-0.001544
0.02	0.8	0.3	0.3	0.4	-0.011863	-0.002332
		0.5			-0.011873	-0.003585
		0.7			-0.011882	-0.005430
0.02	0.8	0.3	0.4	0.4	-0.011859	-0.001617
			0.6		-0.011860	-0.001759
			0.8		-0.011861	-0.001829
0.02	0.8	0.2	0.3	0.5	-0.011857	-0.001221
				0.7	-0.011854	-0.000854
				1.0	-0.011853	-0.000589

Table 4 – Local Nusselt $-\theta'(0)$ and local Sherwood number $-\phi'(0)$ via $k, M, N, Nt, Nb, Pr, \delta t$ and βi_1 when $\lambda = 0.5, \aleph = 0.2, Sc = 0.8, \beta i_2 = 0.5, \alpha =, \beta =, \gamma =, \delta =, \varphi =, \chi =, \psi =, \omega = 1$

k	Nb	Nt	Pr	δc	βi_1	$-\theta'(0)$	$-\phi'(0)$
0.02	0.1	0.1	0.1	0.3	0.5	0.131210	0.170429
	0.1					0.132677	0.172364
	0.2					0.135125	0.175472
	0.3					0.137668	0.178540
0.02	0.2	0.1	0.1	0.3	0.5	0.112657	0.199669
	0.5					0.111522	0.227638
	1.0					0.109666	0.231355
	1.5					0.108024	0.232754
0.02	0.1	0.2	0.1	0.3	0.5	0.117431	0.203830
		0.3				0.125868	0.184735
		0.4				0.142076	0.179484
0.02	0.1	0.1	0.2	0.3	0.5	0.139093	0.196106
			0.5			0.138996	0.175981
			0.6			0.131360	0.170637
0.02	0.1	0.1	0.1	0.4	0.5	0.178637	0.187228
				0.6		0.178646	0.176053
				0.8		0.178657	0.164274
0.02	0.1	0.1	0.1	0.3	0.6	0.138890	0.170074
					0.7	0.144879	0.169514
					1.2	0.162701	0.167324

5 Conclusions

This study presents high order slip flow of non-linear convective of couple stress fluid with nanoparticle past 3D expanding surface. Few summary from the study are:

- Best harmony and valid with preceding numerical result the bvp5c algorithm is appropriate for the solution of the problem
- Transfer of heat is enhanced by the growth of the parameters $Nb, Nt, \beta i_1, \delta_t$
- Heat transfer is diminish with the rise of the parameters N and Pr .
- λ, k, Sc and Nb have similar effects on the profile of concentration.
- The parameters γ and δ playing as a catalysis for the development of skin friction coefficient along x and y-axis.

References

- [1] Srinivasacharya D, Kaladhar K. Mixed convection flow of couple stress fluid between parallel vertical plates with Hall and Ion-slip effects. Communications in Nonlinear Science and Numerical Simulation. 2012;17(6):2447–2462.

- [2] Umavathi J, Chamkha A, Manjula M, Al-Mudhaf A. Flow and heat transfer of a couple-stress fluid sandwiched between viscous fluid layers. *Canadian journal of physics*. 2005;83(7):705–720.
- [3] Hayat T, Aziz A, Muhammad T, Ahmad B. Influence of magnetic field in three-dimensional flow of couple stress nanofluid over a nonlinearly stretching surface with convective condition. *PloS one*. 2015;10(12):e0145332.
- [4] Mahabaleshwar U, Sarris I, Hill AA, Lorenzini G, Pop I. An MHD couple stress fluid due to a perforated sheet undergoing linear stretching with heat transfer. *International Journal of Heat and Mass Transfer*. 2017;105:157–167.
- [5] Ramzan M. Influence of Newtonian heating on three dimensional MHD flow of couple stress nanofluid with viscous dissipation and joule heating. *PloS one*. 2015;10(4):e0124699.
- [6] Ramzan M, Farooq M, Alsaedi A, Hayat T. MHD three-dimensional flow of couple stress fluid with Newtonian heating. *The European Physical Journal Plus*. 2013;128(5):49.
- [7] Adesanya S, Fakoya M. Second law analysis for couple stress fluid flow through a porous medium with constant heat flux. *Entropy*. 2017;19(9):498.
- [8] Ali N, Khan SU, Sajid M, Abbas Z. MHD flow and heat transfer of couple stress fluid over an oscillatory stretching sheet with heat source/sink in porous medium. *Alexandria Engineering Journal*. 2016;55(2):915–924.
- [9] Shit G, Roy M. Hydromagnetic effect on inclined peristaltic flow of a couple stress fluid. *Alexandria Engineering Journal*. 2014;53(4):949–958.
- [10] Ghosh S, Mukhopadhyay S, Hayat T. Couple Stress Effects on Three Dimensional Flow of Magnetite–Water Based Nanofluid Over an Extended Surface in Presence of Non-linear Thermal Radiation. *International Journal of Applied and Computational Mathematics*. 2018;4(1):11.
- [11] Thammanna G, Kumar KG, Gireesha B, Ramesh G, Prasannakumara B. Three dimensional MHD flow of couple stress Casson fluid past an unsteady stretching surface with chemical reaction. *Results in physics*. 2017;7:4104–4110.
- [12] Khan NA, Riaz F, Sultan F. Effects of chemical reaction and magnetic field on a couple stress fluid over a non-linearly stretching sheet. *The European Physical Journal Plus*. 2014;129(1):18.
- [13] Asad S, Alsaedi A, Hayat T. Flow of couple stress fluid with variable thermal conductivity. *Applied Mathematics and Mechanics*. 2016;37(3):315–324.
- [14] Ibrahim W, Gadisa G. Finite element analysis of couple stress micropolar nanofluid flow by non-Fourier’s law heat flux model past stretching surface. *Heat TransferAsian Research*. 2019;48(8):3763–3789.
- [15] Khan NA, Riaz F, Khan NA. Heat transfer analysis for couple stress fluid over a nonlinearly stretching sheet. *Nonlinear Engineering*. 2013;2(3-4):121–127.

- [16] Ibrahim W, Gadisa G. Nonlinear convective boundary layer flow of micropolar-couple stress nanofluids past permeable stretching sheet using Cattaneo-Christov heat and mass flux model. *Heat Transfer*;.
- [17] Shah Z, Kumam P, Dawar A, Alzahrani EO, Thounthong P. Study of the couple stress convective micropolar fluid flow in a hall MHD generator system. *Front Phys* 7: 171 doi: 103389/fphy. 2019;.
- [18] Khan SU, Shehzad SA, Rauf A, Ali N. Mixed convection flow of couple stress nanofluid over oscillatory stretching sheet with heat absorption/generation effects. *Results in physics*. 2018;8:1223–1231.
- [19] Rehman A, Nadeem S, Malik M. Stagnation flow of couple stress nanofluid over an exponentially stretching sheet through a medium. *Journal of Power Technologies*. 2013;93(2):122–132.
- [20] Hayat T, Mustafa M, Iqbal Z, Alsaedi A. Stagnation-point flow of couple stress fluid with melting heat transfer. *Applied Mathematics and Mechanics*. 2013;34(2):167–176.
- [21] Awad F, Haroun N, Sibanda P, Khumalo M. On couple stress effects on unsteady nanofluid flow over stretching surfaces with vanishing nanoparticle flux at the wall. *Journal of Applied Fluid Mechanics*. 2016;9(4):1937–1944.
- [22] Umavathi CJ, Sheremet M. Flow and heat transfer of couple stress nanofluid sandwiched between viscous fluids. *International Journal of Numerical Methods for Heat & Fluid Flow*. 2019;.
- [23] Ellahi R, Zeeshan A, Hussain F, Asadollahi A. Peristaltic blood flow of couple stress fluid suspended with nanoparticles under the influence of chemical reaction and activation energy. *Symmetry*. 2019;11(2):276.
- [24] Sithole H, Mondal H, Goqo S, Sibanda P, Motsa S. Numerical simulation of couple stress nanofluid flow in magneto-porous medium with thermal radiation and a chemical reaction. *Applied Mathematics and Computation*. 2018;339:820–836.
- [25] Rosali H, Ishak A, Nazar R, Pop I. Mixed convection boundary layer flow past a vertical cone embedded in a porous medium subjected to a convective boundary condition. *Propulsion and Power Research*. 2016;5(2):118–122.
- [26] Daniel YS, Aziz ZA, Ismail Z, Salah F. Entropy analysis in electrical magnetohydrodynamic (MHD) flow of nanofluid with effects of thermal radiation, viscous dissipation, and chemical reaction. *Theoretical and Applied Mechanics Letters*. 2017;7(4):235–242.
- [27] Straughan B. Thermal convection with the Cattaneo–Christov model. *International Journal of Heat and Mass Transfer*. 2010;53(1-3):95–98.
- [28] Zhao Q, Xu H, Fan T. Analysis of three-dimensional boundary-layer nanofluid flow and heat transfer over a stretching surface by means of the homotopy analysis method. *Boundary Value Problems*. 2015;2015(1):64.
- [29] Alam MS, Islam MR, Ali M, Alim MA, Alam MM. Magnetohydrodynamic boundary layer flow of non-Newtonian fluid and combined heat and mass transfer about an inclined stretching sheet. *Open Journal of Applied Sciences*. 2015;5(06):279.

- [30] Palwasha Z, Khan NS, Shah Z, Islam S, Bonyah E. Study of two-dimensional boundary layer thin film fluid flow with variable thermo-physical properties in three dimensions space. *AIP Advances*. 2018;8(10):105318.
- [31] Dinesh P, Nalinakshi N, Sandeep N. Double diffusive mixed convection in a couple stress fluids with variable fluid properties. *Adv Physics Theo & Appl*. 2015;41:30–42.
- [32] Malvandi A, Hedayati F, Nobari M. An analytical study on boundary layer flow and heat transfer of nanofluid induced by a non-linearly stretching sheet. *Journal of Applied Fluid Mechanics*. 2014;7(2):375–384.
- [33] Ibrahim W. Three dimensional rotating flow of Powell-Eyring nanofluid with non-Fouriers heat flux and non-Ficks mass flux theory. *Results in physics*. 2018;8:569–577.